



# Geochemical variation at the Hawaiian hot spot caused by upper mantle dynamics and melting of a heterogeneous plume

**Todd Anthony Bianco and Garrett Ito**

*Department of Geology and Geophysics, SOEST, University of Hawai'i at Manoa, Honolulu, Hawaii 96822, USA  
(tbianco@hawaii.edu)*

**Jeroen van Hunen**

*Department of Earth Sciences, Durham University, Durham DH1 3LE, UK*

**Maxim D. Ballmer**

*Institute of Geophysics, ETH Zurich, Zurich CH-8093, Switzerland*

**John J. Mahoney**

*Department of Geology and Geophysics, SOEST, University of Hawai'i at Manoa, Honolulu, Hawaii 96822, USA*

[1] Geochemical variations within the young Hawaiian Islands occur in two particularly prominent forms: differences between volcanic stages and differences between the “Loa” and “Kea” subchains. These observations have been interpreted to reveal spatial patterns of compositional variation in the mantle, such as concentric zoning about the hot spot or elongate streaks along the hot spot track. Our numerical models of a hot plume of upwelling mantle that is interacting with, and melting beneath, a moving lithospheric plate suggest some of the above interpretations should be reevaluated. The mantle plume is assumed to be uniformly isotopically heterogeneous, thus without any compositional zoning. Nonetheless, our models predict geographic zoning in lava isotope composition, an outcome that is caused by differences in melting depths of distinct source components and plume-lithosphere interaction. Isotope compositions of model volcanoes that grow as they pass over the melting zone can explain some of the gross aspects of isotope variation at Hawaii. The results illustrate that chemical zoning at the surface is not necessarily a map of zoning in the mantle, and this affects further inferences about the chemical structure of the mantle.

**Components:** 6790 words, 4 figures.

**Keywords:** mantle; dynamics; heterogeneity; melting; Hawaii; hot spot.

**Index Terms:** 1038 Geochemistry: Mantle processes (3621); 8415 Volcanology: Intra-plate processes (1033, 3615).

**Received** 29 May 2008; **Revised** 15 September 2008; **Accepted** 18 September 2008; **Published** 13 November 2008.

Bianco, T. A., G. Ito, J. van Hunen, M. D. Ballmer, and J. J. Mahoney (2008), Geochemical variation at the Hawaiian hot spot caused by upper mantle dynamics and melting of a heterogeneous plume, *Geochem. Geophys. Geosyst.*, 9, Q11003, doi:10.1029/2008GC002111.



## 1. Introduction: Geochemical Variations at Hot Spots

[2] Temporal and geographic variations in lava geochemistry are observed at prominent hot spots in a variety of tectonic settings, such as Hawaii [e.g., *Tatsumoto*, 1978; *Frey and Rhodes*, 1993; *Lassiter et al.*, 1996; *DePaolo et al.*, 2001; *Regelous et al.*, 2003; *Bryce et al.*, 2005], the Galápagos, [*Geist et al.*, 1988; *Graham et al.*, 1993; *White et al.*, 1993; *Harpp and White*, 2001], and Iceland [*Schilling*, 1973; *Schilling et al.*, 1999; *Breddam et al.*, 2000; *Kokfelt et al.*, 2006]. Previous authors have attributed such geographic trends directly to geographic variations in composition of the solid mantle, which are often thought to be associated with mantle plumes rising through various forms of a chemical layered mantle [e.g., *Hofmann*, 1997].

[3] At Hawaii, for example, isotope data collected from the most voluminous, shield stage of volcanism indicate that this phase is fed by a source characterized by long-term enrichment in highly incompatible elements, whereas later stages of volcanism show evidence for less enrichment in the source [e.g., *Kurz et al.*, 1987, 1996; *Lassiter et al.*, 1996; *DePaolo et al.*, 2001; *Bryce et al.*, 2005]. One hypothesis to explain the compositional difference between the two stages is with a concentrically zoned mantle plume, with an enriched, shield source in the center and a depleted, post-shield source at the periphery [*Frey and Rhodes*, 1993; *Lassiter et al.*, 1996; *Bryce et al.*, 2005]. Concentric zoning may be caused by a rising mantle plume with a center that is composed of material from the deepest mantle and a surrounding sheath that is largely entrained material from the shallower mantle [e.g., *Kurz and Kammer*, 1991; *Frey and Rhodes*, 1993; *Hauri et al.*, 1994; *Lassiter et al.*, 1996].

[4] Isotope data sets also reveal prominent geographical variations within the Hawaiian Islands, the most prominent of which is seen as isotopic distinctions between the subparallel (Mauna) “Loa” volcanic chain (southern line) and (Mauna) “Kea” chain (northern line). Isotope compositions indicate that the line of volcanoes that make up the Loa chain sample a source that has greater long-term enrichment of incompatible elements compared to the source sampled by volcanoes that make up the Kea chain [e.g., *Frey and Rhodes*, 1993; *Kurz et al.*, 1996; *Abouchami et al.*, 2005; *Bryce et al.*, 2005]. The concentrically zoned plume concept may explain these observations if

the two subchains pass over the plume at different distances from the center [*Lassiter et al.*, 1996; *Bryce et al.*, 2005]. Another explanation of the Loa-Kea difference is that the plume has a northeast-southwest asymmetry in composition [*Abouchami et al.*, 2005]. Both the concentric zoning and lateral asymmetry models suggest the plume draws material from deeper-mantle chemical heterogeneities of length scales equal to or larger than that of upwelling itself.

[5] The above interpretations are straightforward, but in order to connect magma composition to the source one must understand the process of magma genesis, which can be complex, particularly in the presence of source heterogeneity [e.g., *Sobolev et al.*, 2007; *Phipps Morgan*, 2001]. Previous authors have proposed that buoyancy-driven upwelling can contribute to the relatively incompatible-element-enriched geochemical signature of hot spot lavas compared to normal mid-ocean ridge basalts [*Kurz and Geist*, 1999; *Breddam et al.*, 2000, *Schilling et al.*, 1999]. Other studies that model melting of small-scale heterogeneities show that erupted magma composition can be influenced strongly by the upwelling pattern in a melting zone [*Bianco et al.*, 2005; *Ito and Mahoney*, 2005a, 2005b, 2006]. We thus anticipate that the complex upper mantle dynamics expected for a mantle plume can lead to surface compositions with geographic patterns that can deviate from any inherent pattern within the mantle source.

[6] This paper examines the 3-D flow and melting of a two-component mantle plume interacting with a moving plate. The source material is nonzoned but is heterogeneous at spatial scales much smaller than the melting zone. This work quantifies the spatial (and temporal) variation of the isotope ratios of magmas that may erupt at the surface and compares these predictions to observations at Hawaii.

## 2. Method: 3-D Dynamics and Nonzoned Mantle

[7] To model the 3-D mantle flow, heat transfer, and melting of the upper mantle, we use the finite element code Citcom [*Moresi and Gurnis*, 1996; *Zhong et al.*, 2000]. The model space spans 1600 km by 800 km horizontally with 6.25 km grid resolution, and is 400 km deep with 5 km resolution (Figure 1a). The extended Boussinesq approximation that we apply includes latent heat due to melting and adiabatic heating, but not viscous dissipation. Viscosity is determined by a temperature-dependent

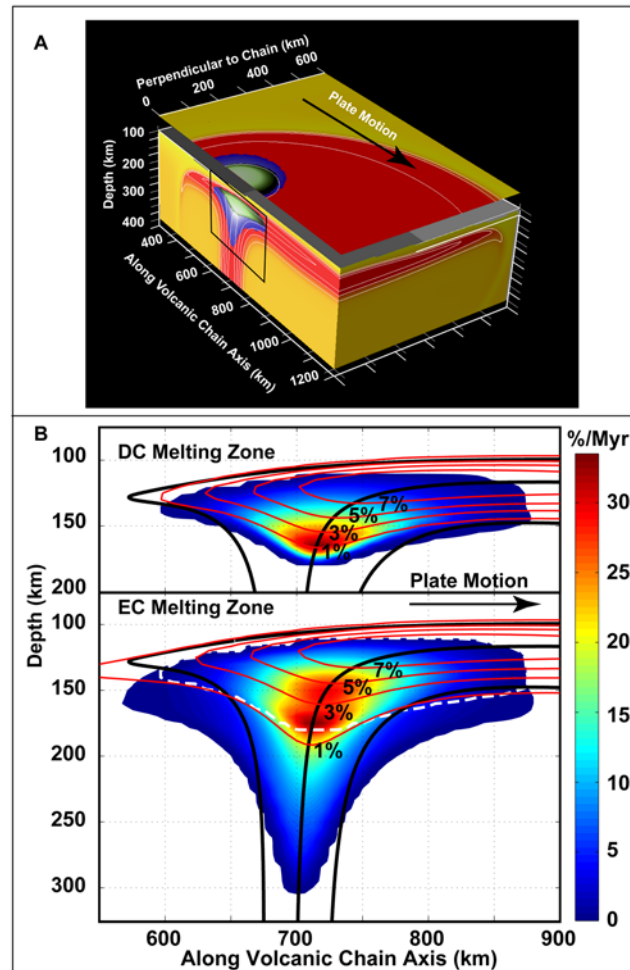


**Figure 1.** (a) Model overview. Slices through the model domain show projections of the 3-D potential temperature field in shades of yellow (cool) and red (warm); the full model domain is 1600 km wide along the volcanic axis, 800 km horizontal and perpendicular to the volcanic axis, and 400 km deep. White contours mark 1350°, 1450°, and 1550°C. The horizontal plane is at a depth of 150 km but plotted above its actual depth for visibility. Black arrow indicates the direction of plate motion. The EC (blue) and DC (green) melting zones are also projected to the horizontal and along-axis slices. The black box outlines area plotted in Figure 1b. (b) Melting zones. Melting rate contours on a vertical slice through the center of the plume (see Figure 1a). The EC and DC melting zones are plotted in different boxes for visibility; however, they exist in the same space (as heterogeneities are much smaller scale than the melting zones and theoretically DC material is veined with EC material) and this is conveyed by the white dashed outline of the DC melting zone plotted over the EC melting zone. Thin red lines are extent of melting contours; the maximum extent of melting is  $\sim 9\%$  for both EC and DC. Thick black lines are particle paths.

Newtonian rheology exactly as described by *Zhong and Watts* [2002] with the exception that the reference viscosity is  $5 \times 10^{19}$  Pa s at the ambient mantle (potential) temperature of 1300°C. The initial temperature condition is the solution of a half-space that has cooled for 100 Ma plus an adiabatic gradient. The bottom boundary temperature condition matches the initial condition plus a circular Gaussian anomaly with a peak excess temperature of 290°C (and decreases by a factor of  $e$  at a radius of 50 km) to form the plume [*Zhong and Watts*, 2002]. The top of the model space is

fixed at 25°C. Maximum vertical velocity in the model is  $\sim 190$  cm/a and the resulting thermal buoyancy flux is 12 Mg/s, which is higher than, but comparable to, other estimates of the Hawaiian anomaly [e.g., *Sleep*, 1992; *Ribe and Christensen*, 1999]. Finally, a horizontal velocity boundary condition ( $\sim 9$  cm/a) is imposed on the top of the model space to simulate plate motion, the vertical wall containing the plume center is a reflecting boundary, and all other boundaries are open to flow with zero conductive heat flow [*Ribe and Christensen*, 1999].

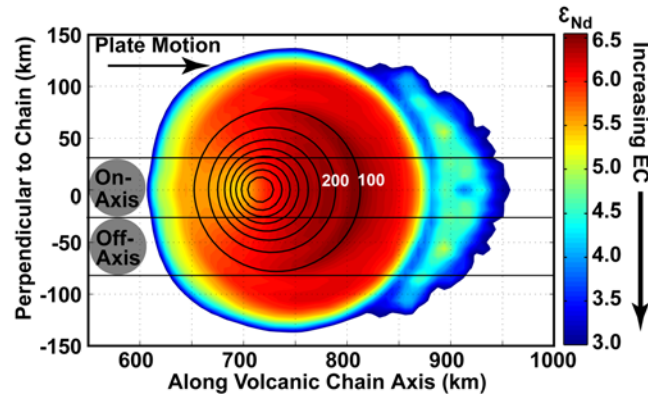


**Figure 2.** Seafloor composition and eruption rate. Map view of model Nd isotope composition (colored as  $\epsilon_{Nd}$ ) assuming EC and DC melts rise vertically and mix perfectly at the surface (see equation (1)). Low  $\epsilon_{Nd}$  (blue) is associated with EC and high  $\epsilon_{Nd}$  (red) is associated with DC. Black contour lines are eruption rates in  $\text{km}^3/\text{Ma}$  (where 100 and 200  $\text{km}^3/\text{Ma}$  are labeled) and the center of these contours is the center of the hot spot. Gray circles are the area from which volcanoes will sample magma, and horizontal lines show the paths that two volcanoes take as they move with the plate.

[8] To model melting, we calculate the extent of melting on the same Eulerian (fixed) mesh used to calculate temperature and pressure using parameterized solidi [Katz *et al.*, 2003]. A passive tracer advection scheme is used to track the total extent of partial melting ( $F$ ) of all solid material in the mantle. Melting rate is the difference between  $F$  calculated at a node and the  $F$  advected to the node during a time step, divided by the time step duration, where refreezing is prohibited ( $\partial F/\partial t \geq 0$ ) [see Ribe and Christensen, 1999, equations (2)–(3)]. The total extent of partial melting also controls the water content (and trace element composition) of both the solid and melt. We adapt the model of Katz *et al.* [2003] to simulate near fractional melting by assuming equilibrium occurs between the solid and melt generated at each time step and that the advected solid composition as a function of  $F$  is that for fractional melting.

[9] In the case presented here, two components are randomly distributed throughout the mantle: 10% enriched peridotite (“EC”) and 90% depleted peridotite (“DC”). EC is enriched in incompatible trace elements and has lower normalized  $^{143}\text{Nd}/^{144}\text{Nd}$ , ( $\epsilon_{Nd} = -3.3$ ) compared to DC (9.8). Also, DC is anhydrous while EC has a water content of 400 ppm, which (using other parameters identical to that in the work of Katz *et al.* [2003]) lowers the EC solidus by  $121^\circ\text{C}$  relative to DC. Thus, the partial melting zones of DC and EC overlap, but melting of EC begins deeper, is wider, and continues to higher maximum extents (Figure 1b). We assume the components equilibrate thermally with each other, but remain chemically separate [e.g., Phipps Morgan, 2001]. To predict magma

composition, we assume magma (from both components) rises vertically to the surface and mixes (or pools) in direct proportion to the rate generated in the mantle. The composition of magma that has risen to the to the seafloor (Figure 2) is thus

$$\epsilon_{Nd}(x, y) = \frac{\sum_{l=1}^2 \sum_{n=1}^N \epsilon_{Nd}^l \phi^l C_o^l E_n^l (\partial F_n^l / \partial t)}{\sum_{l=1}^2 \sum_{n=1}^N \phi^l C_o^l E_n^l (\partial F_n^l / \partial t)} \quad (1)$$

where the finite element mesh is uniform,  $l$  is the lithology (EC or DC),  $n$  is the depth position of a finite element grid point,  $N$  is the number of vertical grid points, and  $\epsilon_{Nd}^l$ ,  $\phi^l$ , and  $C_o^l$  are the  $\epsilon_{Nd}$  composition, the starting mantle mass fraction, and the initial Nd concentration of a lithology, respectively. The function  $E_n^l$  is the factor enrichment of the Nd in the magma, relative to the starting solid ( $C_o^l$ ) as given by the fractional melting equation and  $\partial F_n^l / \partial t$  is the melting rate at a grid point. The assumptions made in equation (1) are most valid if real mantle melting is fractional [Johnson *et al.*, 1990; Langmuir *et al.*, 1992; McKenzie, 2000; Rubin *et al.*, 2005] or if any potential liquid-solid interactions do not affect the relative melt generation rates in the mantle. Indeed there is evidence that mantle melt transport is rapid and/or fractional.

### 3. Results: Predicted Geochemical Trends

[10] The prediction (Figure 2) is that melting a uniformly heterogeneous mantle plume can result



in compositional zoning at the surface. At the very edges of the melting zone, EC is the only material melting and thus expressed at the surface. Over a broad area within these outer edges, compositions have higher  $\epsilon_{Nd}$ , which is where DC melting is productive. Near to where the magma flux is greatest (at an along-chain distance of  $x = 675\text{--}700$  km), a local minimum in  $\epsilon_{Nd}$  (local maximum in EC) occurs. This minimum reflects efficient EC melting near the center of the plume stem where the EC melting zone extends deepest beneath the DC melt zone and where active upwelling is fastest within the EC melting zone. Overall, the magmatic geochemical pattern resembles a form of radial zoning with an EC-like center surrounded by a broad zone with stronger DC-type compositions and a thin EC-rich rim.

[11] In addition, the pattern is considerably asymmetric in the direction of plate motion, with more EC-like compositions upstream of plate motion than downstream. This is caused by shearing of the rising plume by plate motion. Shearing offsets the most productive central portion of the DC melting zone slightly downstream from that of the EC zone. The tilting of the center streamline in Figure 1b gives a sense of this effect. Also, shearing causes both melting zones to extend less far upstream of the center streamline than downstream, but this effect is greater for the DC melting zone because it is shallower. The net result is a higher flux of melts from EC than from DC on the upstream side than farther downstream as reflected in the surface pattern in Figure 2. Increasing lithospheric thickness and plate speed tends to increase the asymmetry of the pattern, increasing Rayleigh number tends to decrease the asymmetry.

[12] We now predict the composition of volcanoes formed by passage of the plate over the model mantle and compare these predictions to specific data sets collected at Hawaii. Here we assume that the circular area over which a volcano samples magma has a constant radius (25 km) as it moves with the plate over the hot spot (see Figure 2). An extensive data set on the evolution of a single volcano from the midshield stage to later stages comes from the Hawaii Scientific Drilling Project (HSDP). Figure 3 shows both predicted and observed  $\epsilon_{Nd}$  versus the percent of the total volcano thickness. Thickness from our models has been computed by assuming that the magma feeding the volcano builds an axisymmetric, cone-shaped volcano [DePaolo and Stolper, 1996] so that we can most easily compare it to HSDP data. Using

fractional thickness allows us compare predictions and compositions at approximately the same stage of volcanism for different locations with different absolute thicknesses.

[13] Figure 3 shows that as the model volcano grows, composition indeed shifts from EC-like to DC-like. The very base of a volcano forms while it is sampling the upstream edge of the melting zone, where virtually only EC is melting and where  $\epsilon_{Nd}$  is low. Between the 10% and 20% range of a volcano's final thickness,  $\epsilon_{Nd}$  rapidly rises, which signals the onset of appreciable DC melting. Above  $\sim 30\%$  of the total thickness, compositions shift more gradually toward higher  $\epsilon_{Nd}$ . This portion of the volcano is being built as the volcano begins to pass into the higher  $\epsilon_{Nd}$  (orange red in Figure 2) portion of the melting zone, while still sampling low  $\epsilon_{Nd}$  (yellow) magma. The simple volcano growth model [DePaolo and Stolper, 1996] predicts volcano thickness to accumulate nonlinearly with volcano volume. This nonlinearity plus the changing eruption rates along the volcano's path cause the transition from moderate (yellow) to intermediate (red)  $\epsilon_{Nd}$  over a considerable part of the shallowest portion of the volcano, which is likely sampled by HSDP. The very last lavas to erupt reveal the low  $\epsilon_{Nd}$  compositions predicted at the very downstream edge of the melting zone. Finally, Figure 3 also illustrates that a volcano passing 50 km off-axis is predicted to have higher  $\epsilon_{Nd}$  values than an on-axis volcano throughout most of the volcano's growth. The explanation is that the on-axis volcano passes directly over the local  $\epsilon_{Nd}$  minimum near the plume center, whereas the off-axis volcano passes largely to the side of this EC-rich melting zone (Figure 2).

[14] The predictions capture some important observed trends at Hawaii. The predicted shift from moderate to high  $\epsilon_{Nd}$  as a function of age for both on- and off-axis model volcanoes follows the prominent trends observed in data from the Mauna Kea section of the HSDP and the combined series of Kilauea, to Kohala shield, to Kohala postshield; the same is true for much of the combined series of the Mauna Loa (except for the shallowest samples) and Koolau, to West Molokai shield, to West Molokai postshield. However, while samples from a Koolau drill core [Salters et al., 2006] overlap with Mauna Loa data, some late shield eruptions on Koolau extend to much lower  $\epsilon_{Nd}$  [Rodden et al., 1994] (not shown in Figure 3), which the model does not predict. Also, the compositional distinction between the shield stages of Loa and Kea

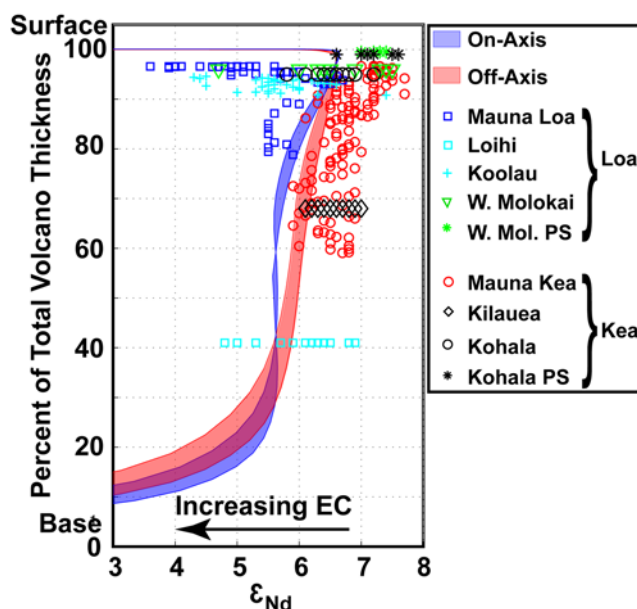


**Figure 3.** Composition versus thickness. Shaded regions show the range of predicted average  $\epsilon_{Nd}$  composition of an on- (blue) and off-axis (red) volcano (see Figure 2), for cone-shaped volcanoes that encompass a range of slopes near those of Hawaiian shields [DePaolo and Stolper, 1996]. The vertical axis is percent of maximum thickness, such that zero is the base of a volcano and 100% is the surface of a fully grown volcano (i.e., for a 10 km thick, extinct volcano, 20% represents surface 2 km above the base). Colored shapes are data for Mauna Loa (blue squares), Loihi (cyan squares), Koolau (cyan crosses), West Molokai (green triangles), West Molokai postshield (green stars), Mauna Kea (red circles), Kilauea (black diamonds), Kohala (black circles), and Kohala postshield (black stars) (see GEOROC database <http://georoc.mpch-mainz.gwdg.de> and references therein; Koolau data from *Salters et al.* [2006]). To plot Mauna Kea and Mauna Loa data on this vertical axis, we normalized the sample depths (or heights for some cases) to 7.5 km and Koolau data is normalized to 6.5 km, the approximate thickness of the volcanoes at the sample locations [see *Wessel*, 1993; *Kurz et al.*, 1995; *Haskins and Garcia*, 2004; *Garcia et al.*, 2007]. Kilauea and Loihi are plotted on the diagram based on the assumption that they erupted 25% and 5% of their final volumes, respectively, consistent with their estimated ages and volumes compared to the duration of most Hawaiian volcanoes [Lipman et al., 2006; Robinson and Eakins, 2006]. Therefore, data collected at the current surface of Kilauea plot at the same thickness as data collected deep in a Mauna Kea drill core. Estimated volumes, ages, or depths are not available for West Molokai or Kohala, so we assumed these samples occurred at volume percentages that typify the end of the corresponding stages: 95% for shield data and 99% for postshield data.

subchain volcanoes is captured by the sustained  $\epsilon_{Nd}$  difference between the on- and off-axis model volcanoes, which is a concept proposed by other workers [e.g., *Lassiter et al.*, 1996, *Bryce et al.*, 2005]. Then, after  $\sim 95\%$  of the total crust has erupted, this compositional distinction is predicted to end because of the concentric like compositional pattern (see Figure 2). This prediction may explain why postshield data from West Molokai (on the Loa subchain) overlaps with postshield data from Mauna Kea and Kohala (on the Kea subchain). However, late-shield and postshield data from other Loa subchain volcanoes (e.g., Hualalai, Kahoolawe, and Koolau) do preserve a distinction from Kea-like compositions. Finally, compositions of different volcanoes along the Kea subchain overlap each other at the same interpolated thicknesses (e.g., Kilauea erupts the same  $\epsilon_{Nd}$  compo-

sition as deep Mauna Kea lavas). This overlap indicates that the volcanoes erupted the same  $\epsilon_{Nd}$  composition when they occupied the same position over the hot spot, and this is captured in our (and others', e.g., *Abouchami et al.* [2005]; *Bryce et al.* [2005]) steady state model(s). Our model compositions do overlap with Loihi data but the high  $\epsilon_{Nd}$  lavas are not predicted, nor is the range of  $\epsilon_{Nd}$  at Loihi predicted.

#### 4. Discussion

[15] The model presented above predicts large-scale, persistent, geographic variations in isotope composition at Hawaii that are similar to observed trends. However, some potentially important aspects are not included in this initial model. One large simplification is the assumption of a mantle



with only two components (EC and DC), whereas it is widely recognized that three or more components are required to fully explain Hawaii data [e.g., Kurz and Kammer, 1991; Eisele et al., 2003, Abouchami et al., 2005].

[16] Pb-isotope data provide a good constraint on the number of components and style of heterogeneity in the mantle, and successful models should address these data. Recent high-precision Pb-isotope data show that compositions of the Kea and Loa subchains form statistically different populations in  $^{208}\text{Pb}/^{204}\text{Pb}$  versus  $^{206}\text{Pb}/^{204}\text{Pb}$  space [Abouchami et al., 2005]. These authors interpreted the results as indicating that the two subchains sample mutually exclusive, bilateral mantle sources, requiring at least four components beneath Hawaii (two for each subchain). However, the Pb isotope mixing arrays from individual volcanoes do cross with those from the other subchain, which suggests the sources of the subchains are, in fact, not mutually exclusive [Xu et al., 2007]. It may therefore be possible for nonzoned, heterogeneous mantle to explain these data, but with an added third component. Previous calculations showed that a large range of Pb-isotope data can be explained by melting two source types plus varying amounts of a third type [Ito and Mahoney, 2005a, 2005b]. It is possible that a third component is being undersampled by one Hawaiian subchain and more heavily expressed in the other due to differences in the proximity to the center of the plume track much like the behavior of the current two-component models. Regardless of number of components, the model predictions are symmetric across the plume axis, and we, like others before [e.g., Lassiter et al., 1996; Bryce et al., 2005] must assume the axis between the subchains is shifted to the north of the center of the plume to explain differences between the Loa and Kea subchains.

[17] A third component may also help address the discrepancy that the low  $\epsilon_{\text{Nd}}$  values predicted during the early growth of both on- and off-axis volcanoes fall on the low end of the range measured at Loihi. A suitable component may have, relative to global values, intermediate  $^{87}\text{Sr}/^{86}\text{Sr}$ ,  $\epsilon_{\text{Nd}}$  and high  $^3\text{He}/^4\text{He}$  [Kurz et al., 1996], much like the proposed “C” [Hanan and Graham, 1996] or “FOZO” [Hart et al., 1992] components. Because our model predicts the earliest lava composition to be dominated by the deepest-melting lithology, a small amount of a deep-melting, C-like component (with  $\epsilon_{\text{Nd}} \approx 6$ ) might improve the match to the Loihi  $\epsilon_{\text{Nd}}$  values. It might also explain

the high  $^3\text{He}/^4\text{He}$  values for Loihi (as high as 32 times atmospheric  $^3\text{He}/^4\text{He}$ ), which provide another line of evidence for more than two components.

[18] Another weakness of our dynamic models deals with the well-known evolution of major element composition from the tholeiitic lavas erupted during the shield phase to the more alkalic lavas erupted during the postshield phase. This tholeiitic-alkalic transition probably represents a change from higher to lower extents of partial melting [e.g., Macdonald and Katsura, 1964; Frey et al., 1990]. We predict the pooled mean extent of partial melting sampled by a volcano as

$$\bar{F} = \frac{\sum_{l=1}^2 \sum_{n=1}^N F_n^l \phi^l (\partial F_n^l / dt)}{\sum_{l=1}^2 \sum_{n=1}^N \phi^l (\partial F_n^l / dt)} \quad (2)$$

for a uniform mesh, where  $F$  is the extent of partial melting and in this case  $n$  is the position of a grid point and is summed over  $N$  nodes inside a cylindrical capture volume beneath the volcano (see Figure 2). Figure 4 shows that predicted mean extent of partial melting,  $\bar{F}$  increases (or remains high) with distance along the plume track until >99% of the total melt volume is produced. This prediction is inconsistent with the observation of alkalic post-shield lavas in the last  $\sim 2.5\%$  of the total erupted volume [Frey et al., 1990] as well as with the general association of postshield alkalic lavas and “depleted” (e.g., high- $\epsilon_{\text{Nd}}$ ) isotope compositions [e.g., Chen and Frey, 1985; Frey et al., 1990; Kennedy et al., 1991; Feigenson et al., 2003].

[19] The model prediction of late-stage high  $\bar{F}$  is caused by the solid residue near the center of the hot spot being swept with plate motion and continuing to melt to higher fractions on the downstream end of the melting zone. It is a result that is not predicted in parameterized models of concentric melting zones that do not consider plate shear [e.g., Lassiter et al., 1996; Bryce et al., 2005]. This behavior is independent of any of our isotope calculations or whether two or even a single source component is present, and we have not seen a dynamical model of a plume beneath a moving plate that adequately predicts such low  $\bar{F}$  in the appropriate location on the downstream end of the melting zone. This result presents a new challenge for all dynamical models of plume-plate interaction to explain.

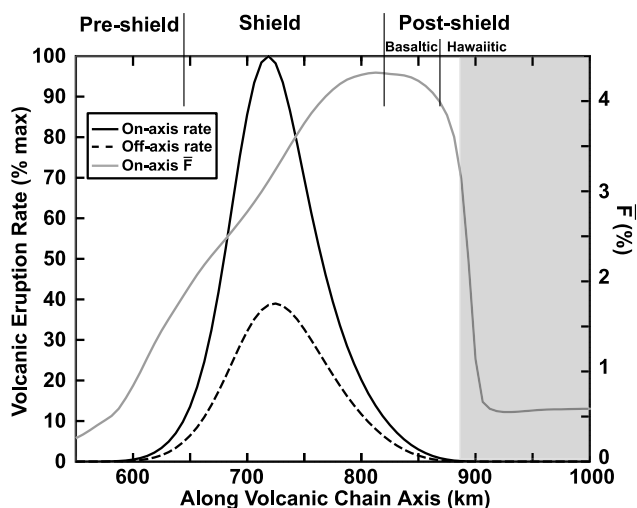


**Figure 4.** Eruption rate and  $\bar{F}$ . Heavy black lines mark eruption rates for an on-plume-axis volcano (solid) and an off-axis volcano (dashed), normalized to the maximum rate of the on-axis volcano,  $\sim 36 \times 10^6 \text{ m}^3/\text{a}$ . Rates are the sum of melting rates in vertical cylindrical capture areas passing over the hot spot (see Figure 2). The solid gray line is mean extent of melting  $\bar{F}$  (see equation (2)) for an on-axis volcano. Vertical black lines indicate the approximate volume fractions (applicable to both on- and off-axis volcanoes) that delineate the preshield and postshield stages of Mauna Kea [see Frey *et al.*, 1990, and references therein]. Postshield, alkalic stages began at Mauna Kea when volume rates fell to 10% of the maximum, and these stages account for  $\sim 2.5\%$  of the total erupted magma. In contrast, a ( $>1\%$ ) decrease of  $\bar{F}$  in the model (gray box), which we use as a qualitative proxy for the onset of alkalic magma production, occurs when volume fluxes and total volume fall well below 1% of the maxima. This inconsistency occurs regardless of whether we melt a one- (not shown) or two-component (gray curve) mantle; it is a new issue that needs to be addressed by any dynamic model of plume-plate interaction. In this model peak eruption rate is  $\sim 36 \times 10^6 \text{ m}^3/\text{a}$  on-axis and  $14 \times 10^6 \text{ m}^3/\text{a}$  off-axis, and total erupted volume is  $\sim 4.0 \times 10^4 \text{ km}^3$  on-axis and  $1.7 \times 10^4 \text{ km}^3$  off-axis. The prediction that on-axis volcanoes erupt more than double the peak rate and total volume of off-axis volcanoes is consistent with estimates that Mauna Loa is nearly double the volume of Mauna Kea but inconsistent with small differences in erupted volumes estimated at other Loa and Kea subchain volcanoes [DePaolo and Stolper, 1996; Robinson and Eakins, 2006].

[20] The most robust finding of this study, regardless of its specific application to Hawaii, is that the coupling of upper mantle dynamics and melting of small-scale mantle heterogeneities can lead to larger-scale geographic compositional variations at the surface. The broader implication is that if any compositional zoning is present in a plume at spatial scales comparable to the scales of the plume itself, such as that caused by a plume entraining ambient mantle as it rises through a layered mantle, then the zoning could be less substantial or quite different than previously inferred for Hawaii or other hot spots. Consideration of the upper mantle dynamics as done here is therefore essential for inferring the composition of the mantle from which plumes originate and through which they rise. Our model also predicts that if plumes contain streaks or blobs of heterogeneity [e.g., Farnetani *et al.*, 2002; Eisele *et al.*, 2003; Abouchami *et al.*, 2005; Farnetani and Samuel, 2005; Marske *et al.*, 2007], the sampling of such heterogeneity will not be constant over the life of a volcano, even if the

mass fraction of heterogeneity entering the melting zone is constant. A logical step for future work is to include the dynamic effects illustrated in this study with different forms of zoning in the source to see if they can better explain the data than the current model.

## 5. Conclusions

[21] Upper mantle dynamics and melting of a heterogeneous source can lead to strong geographical variations in the isotope composition of magmas erupted at the surface, independent of any geographical variation in mantle source. Our model of an intraplate plume predicts Nd-isotope compositions that change from the center to the end of the melting zone in the same sense as that recorded by the shield to postshield progression of Hawaiian volcanoes. If volcanoes pass at different distances from the hot spot center, our model also predicts compositions that are consistent with the sustained differences between Loa (on-axis) and Kea (off-



axis) subchains. These results offer an alternative explanation for these well-established observations at Hawaii. Finally, our results motivate reevaluations of the amplitude or even presence of compositional zoning in plumes and the mantle through which plumes rise beneath Hawaii and other hot spots.

## Acknowledgments

[22] We thank D. DePaolo, M. Garcia, J. Dixon, D. Weis, and two anonymous reviewers for various discussions that helped improved this manuscript. Ito, Mahoney, and Bianco were supported by NSF-CSEDI grant 0440365. This is SOEST contribution 7561.

## References

- Abouchami, W., A. W. Hofmann, J. G. Galer, F. A. Frey, J. Eisele, and M. Feigenson (2005), Lead isotopes reveal bilateral asymmetry and vertical continuity in the Hawaiian mantle plume, *Nature*, *434*, 851–856.
- Bianco, T. A., G. Ito, J. M. Becker, and M. O. Garcia (2005), Secondary Hawaiian volcanism formed by flexural arch decompression, *Geochem. Geophys. Geosyst.*, *6*, Q08009, doi:10.1029/2005GC000945.
- Breddam, K., M. D. Kurz, and M. Storey (2000), Mapping out the conduit of the Iceland mantle plume with helium isotopes, *Earth Planet. Sci. Lett.*, *176*, 45–55, doi:10.1016/S0012-821X(99)00313-1.
- Bryce, J. G., D. J. DePaolo, and J. C. Lassiter (2005), Geochemical structure of the Hawaiian plume: Sr, Nd, and Os isotopes in the 2.8 km HSDP-2 section of Mauna Kea volcano, *Geochem. Geophys. Geosyst.*, *6*, Q09G18, doi:10.1029/2004GC000809.
- Chen, C.-Y., and F. A. Frey (1985), Trace element and isotopic geochemistry of lavas from Haleakala volcano, East Maui, Hawaii: Implications for the origin of Hawaiian basalts, *J. Geophys. Res.*, *90*, 8743–8768, doi:10.1029/JB090iB10p08743.
- DePaolo, D. J., and E. M. Stolper (1996), Models of Hawaiian volcano growth and plume structure: Implications of results from the Hawaii Scientific Drilling Project, *J. Geophys. Res.*, *101*, 11,643–11,654, doi:10.1029/96JB00070.
- DePaolo, D. J., J. G. Bryce, A. Dodson, D. L. Shuster, and B. M. Kennedy (2001), Isotopic evolution of Mauna Loa and the chemical structure of the Hawaiian plume, *Geochem. Geophys. Geosyst.*, *2*, 1044, doi:10.1029/2000GC000139.
- Eisele, J., W. Abouchami, J. G. Galer, and A. W. Hofmann (2003), The 320 kyr Pb isotope evolution of Mauna Kea lavas recorded in the HSDP-2 drill core, *Geochem. Geophys. Geosyst.*, *4*(7), 8710, doi:10.1029/2002GC000339.
- Farnetani, C. G., and H. Samuel (2005), Beyond the thermal plume paradigm, *Geophys. Res. Lett.*, *32*, L07311, doi:10.1029/2005GL022360.
- Farnetani, C. G., B. Legras, and P. J. Tackley (2002), Mixing deformations in mantle plumes, *Earth Planet. Sci. Lett.*, *196*, 1–15, doi:10.1016/S0012-821X(01)00597-0.
- Feigenson, M., L. L. Bogle, M. J. Carr, and C. T. Herzberg (2003), REE inverse modeling of HSDP2 basalts: Evidence for multiple sources in the Hawaiian plume, *Geochem. Geophys. Geosyst.*, *4*(2), 8706, doi:10.1029/2001GC000271.
- Frey, F. A., and J. M. Rhodes (1993), Intershield geochemical differences among Hawaiian volcanoes: Implications for source compositions, melting process and magma ascent paths, *Philos. Trans. R. Soc. London, Ser. A*, *342*, 121–136, doi:10.1098/rsta.1993.0009.
- Frey, F. A., W. S. Wise, M. O. Garcia, H. West, S.-T. Kwon, and A. Kennedy (1990), Evolution of Mauna Kea volcano, Hawaii: Petrologic and geochemical constraints on post-shield volcanism, *J. Geophys. Res.*, *95*, 1271–1300, doi:10.1029/JB095iB02p01271.
- Garcia, M. O., E. H. Haskins, E. M. Stolper, and M. B. Baker (2007), Stratigraphy of the Hawaii Scientific Drilling Project core (HSDP2), Anatomy of a Hawaiian shield volcano, *Geochem. Geophys. Geosyst.*, *8*, Q02G20, doi:10.1029/2006GC001379.
- Geist, D. J., W. M. White, and A. R. McBirney (1988), Plume-aesthenosphere mixing beneath the Galapagos archipelago, *Nature*, *333*, 657–660, doi:10.1038/333657a0.
- Graham, D. W., D. M. Christi, K. S. Harpp, and J. E. Lupton (1993), Mantle plume helium in submarine basalts from the Galapagos platform, *Science*, *262*, 2023–2026, doi:10.1126/science.262.5142.2023.
- Hanan, B. B., and D. W. Graham (1996), Lead and helium isotope evidence from oceanic basalts for a common deep source of mantle plumes, *Science*, *272*, 991–995, doi:10.1126/science.272.5264.991.
- Harpp, K. S., and W. M. White (2001), Tracing a mantle plume: Isotopic and trace element variations of Galapagos seamounts, *Geochem. Geophys. Geosyst.*, *2*(6), 1042, doi:10.1029/2000GC000137.
- Hart, S. R., E. H. Hauri, L. A. Oschmann, and J. A. Whitehead (1992), Mantle plumes and entrainment: Isotopic evidence, *Science*, *256*, 517–520, doi:10.1126/science.256.5056.517.
- Haskins, E. H., and M. O. Garcia (2004), Scientific drilling reveals geochemical heterogeneity within the Koolau shield, Hawaii, *Contrib. Mineral. Petrol.*, *147*, 162–188.
- Hauri, E. H., J. A. Whitehead, and S. R. Hart (1994), Fluid dynamic and geochemical aspects of entrainment in mantle plumes, *J. Geophys. Res.*, *99*, 24,275–24,300, doi:10.1029/94JB01257.
- Hofmann, A. W. (1997), Mantle geochemistry: The message from oceanic volcanism, *Nature*, *385*, 219–229, doi:10.1038/385219a0.
- Ito, G., and J. J. Mahoney (2005a), Flow and melting of a heterogeneous mantle: 1. Method and importance to the geochemistry of ocean island and mid-ocean ridge basalts, *Earth Planet. Sci. Lett.*, *230*, 29–46, doi:10.1016/j.epsl.2004.10.035.
- Ito, G., and J. J. Mahoney (2005b), Flow and melting of a heterogeneous mantle: 2. Implications for a chemically non-layered mantle, *Earth Planet. Sci. Lett.*, *230*, 47–63, doi:10.1016/j.epsl.2004.10.034.
- Ito, G., and J. J. Mahoney (2006), Melting a high <sup>3</sup>He/<sup>4</sup>He source in a heterogeneous mantle, *Geochem. Geophys. Geosyst.*, *7*, Q05010, doi:10.1029/2005GC001158.
- Johnson, K. T., H. J. B. Dick, and N. Shimizu (1990), Melting in the oceanic upper mantle: An ion microprobe study of diopsides in abyssal peridotites, *J. Geophys. Res.*, *95*, 2661–2678, doi:10.1029/JB095iB03p02661.
- Katz, R. F., M. Spiegelman, and C. H. Langmuir (2003), A new parameterization of hydrous mantle melting, *Geochem. Geophys. Geosyst.*, *4*(9), 1073, doi:10.1029/2002GC000433.
- Kennedy, A., S.-T. Kwon, F. A. Frey, and H. West (1991), The isotopic composition of postshield lavas from Mauna Kea volcano, Hawaii, *Earth Planet. Sci. Lett.*, *103*, 339–353, doi:10.1016/0012-821X(91)90171-D.
- Kokfelt, T. F., K. Hoernle, F. Haufl, J. Fiebig, R. Werner, and D. Garbe-Schonberg (2006), Combined trace element and Pb-Nd-Sr-O isotope evidence for recycled oceanic crust



- (upper and lower) in the Iceland mantle plume, *J. Petrol.*, *47*, 1705–1749, doi:10.1093/petrology/egl025.
- Kurz, M. D., and D. J. Geist (1999), Dynamics of the Galapagos hotspot from helium isotope geochemistry, *Geochim. Cosmochim. Acta*, *63*, 4139–4156, doi:10.1016/S0016-7037(99)00314-2.
- Kurz, M. D., and D. P. Kammer (1991), Isotopic evolution of Mauna Loa volcano, *Earth Planet. Sci. Lett.*, *103*, 257–269, doi:10.1016/0012-821X(91)90165-E.
- Kurz, M. D., M. O. Garcia, F. A. Frey, and P. A. O'Brien (1987), Temporal helium isotopic variations within Hawaiian volcanoes: Basalts from Mauna Loa and Haleakala, *Geochim. Cosmochim. Acta*, *51*, 2905–2914, doi:10.1016/0016-7037(87)90366-8.
- Kurz, M. D., T. C. Kenna, D. P. Kammer, J. M. Rhodes, and M. O. Garcia (1995), Isotopic evolution of Mauna Loa Volcano: A view from the submarine southwest rift zone, in *Mauna Loa Revealed: Structure, Composition, History, and Hazards*, *Geophys. Monogr. Ser.*, vol. 92, edited by J. M. Rhodes and J. P. Lockwood, pp. 289–306, AGU, Washington, D. C.
- Kurz, M. D., T. C. Kenna, J. C. Lassiter, and D. J. DePaolo (1996), Helium isotopic evolution of Mauna Kea volcano: First results from the 1-km drill core, *J. Geophys. Res.*, *101*, 11,781–11,791, doi:10.1029/95JB03345.
- Langmuir, C. H., E. M. Klein, and T. Plank (1992), Petrologic systematics of mid-ocean ridge basalts: Constraints on melt generation beneath ocean ridges, in *Mantle Flow and Melt Generation at Mid-Ocean Ridges*, *Geophys. Monogr. Ser.*, vol. 71, edited by J. Phipps Morgan, D. K. Blackman, and J. M. Sinton, pp. 183–280, AGU, Washington, D. C.
- Lassiter, J. C., D. J. DePaolo, and M. Tatsumoto (1996), Isotopic evolution of Mauna Kea volcano: Results from the initial phase of the Hawaii Scientific Drilling Project, *J. Geophys. Res.*, *101*, 11,769–11,780, doi:10.1029/96JB00181.
- Lipman, P. W., T. W. Sisson, M. L. Coombs, A. Clavert, and J.-I. Kimura (2006), Piggyback tectonics: Long-term growth of Kilauea on the south flank of Mauna Loa, *J. Volcanol. Geotherm. Res.*, *151*, 73–108, doi:10.1016/j.jvolgeoes.2005.07.032.
- Macdonald, G. A., and T. Katsura (1964), Chemical composition of Hawaiian Lavas, *J. Petrol.*, *5*, 82–133.
- Marske, J. P., A. J. Pietruszka, D. Weis, M. O. Garcia, and J. M. Rhodes (2007), Rapid passage of small-scale mantle heterogeneity through melting regions of Kilauea and Mauna Loa Volcanoes, *Earth Planet. Sci. Lett.*, *259*, 34–50, doi:10.1016/j.epsl.2007.04.026.
- McKenzie, D. P. (2000), Constraints on melt generation and transport from U-series activity ratios, *Chem. Geol.*, *162*, 81–94, doi:10.1016/S0009-2541(99)00126-6.
- Moresi, L., and M. Gurnis (1996), Constraints on the lateral strength of slabs from three-dimensional dynamic flow models, *Earth Planet. Sci. Lett.*, *138*, 15–28, doi:10.1016/0012-821X(95)00221-W.
- Phipps Morgan, J. (2001), Thermodynamics of pressure release melting of a veined plum pudding mantle, *Geochem. Geophys. Geosyst.*, *2*(4), 1001, doi:10.1029/2000GC000049.
- Regelous, M., A. W. Hofmann, W. Abouchami, and J. G. Galer (2003), Geochemistry of lavas from the Emperor seamounts, and the geochemical evolution of Hawaiian magmatism from 85 to 42 Ma, *J. Petrol.*, *44*, 113–140, doi:10.1093/petrology/44.1.113.
- Ribe, N. M., and U. R. Christensen (1999), The dynamical origin of Hawaiian volcanism, *Earth Planet. Sci. Lett.*, *171*, 517–531, doi:10.1016/S0012-821X(99)00179-X.
- Robinson, J. E., and B. W. Eakins (2006), Calculated volumes of individual shield volcanoes at the young end of the Hawaiian ridge, *J. Volcanol. Geotherm. Res.*, *151*, 309–317, doi:10.1016/j.jvolgeoes.2005.07.033.
- Roden, M. F., T. W. Trull, S. R. Hart, and F. A. Frey (1994), New He, Nd, Pb, and Sr isotopic constraints on the constitution of the Hawaiian plume: Results from Koolau volcano, Oahu, Hawaii, USA, *Geochim. Cosmochim. Acta*, *58*, 1431–1440.
- Rubin, K. H., I. Van der Zander, M. C. Smith, and E. C. Bergmanis (2005), Minimum speed limit for ocean ridge magmatism from <sup>210</sup>Pb–<sup>226</sup>Ra–<sup>230</sup>Th disequilibrium, *Nature*, *437*, 534–538, doi:10.1038/nature03993.
- Salter, V. J. M., J. Blichert-Toft, Z. Fekiacova, A. Sachi-Kocher, and M. Bizmis (2006), Isotope and trace element evidence for depleted lithosphere in the source of Koolau basalts, *Contrib. Mineral. Petrol.*, *151*, 297–312, doi:10.1007/s00410-005-0059-y.
- Schilling, J.-G. (1973), Iceland mantle plume: Geochemical study of Reykjanes ridge, *Nature*, *242*, 565–571, doi:10.1038/242565a0.
- Schilling, J.-G., R. Kingsley, D. Fontignie, R. Poreda, and S. Xue (1999), Dispersion of the Jan Mayen and Iceland mantle plumes in the Arctic: A He-Pb-Nd-Sr isotope tracers study of basalts from the Kolbeinsey, Mohns, and Knipovich ridges, *J. Geophys. Res.*, *104*, 10,543–10,569, doi:10.1029/1999JB900057.
- Sleep, N. H. (1992), Hotspots and mantle plumes: Some phenomenology, *J. Geophys. Res.*, *95*, 6715–6737.
- Sobolev, A. V., et al. (2007), The amount of recycled crust in sources of mantle-derived melts, *Science*, *316*, 412–417, doi:10.1126/science.1138113.
- Tatsumoto, M. (1978), Isotopic composition of lead in oceanic basalt and its implication to mantle evolution, *Earth Planet. Sci. Lett.*, *38*, 63–87, doi:10.1016/0012-821X(78)90126-7.
- Wessel, P. (1993), A reexamination of the flexural deformation beneath the Hawaiian Islands, *J. Geophys. Res.*, *98*, 12,177–12,190, doi:10.1029/93JB00523.
- White, W. M., A. R. McBirney, and R. A. Duncan (1993), Petrology and geochemistry of the Galapagos Islands: Portrait of a pathological mantle plume, *J. Geophys. Res.*, *98*, 19,533–19,563, doi:10.1029/93JB02018.
- Xu, G., F. A. Frey, D. A. Clague, W. Abouchami, J. Blichert-Toft, B. Cousens, and M. Weisler (2007), Geochemical characteristics of West Molokai shield- and postshield-stage lavas: Constraints on Hawaiian plume models, *Geochem. Geophys. Geosyst.*, *8*, Q08G21, doi:10.1029/2006GC001554.
- Zhong, S., and A. B. Watts (2002), Constraints on the dynamics of mantle plumes from the uplift of Hawaiian islands, *Earth Planet. Sci. Lett.*, *203*, 105–116, doi:10.1016/S0012-821X(02)00845-2.
- Zhong, S., M. T. Zuber, L. Moresi, and M. Gurnis (2000), Role of temperature-dependent viscosity and surface plates in spherical shell models of mantle convection, *J. Geophys. Res.*, *105*, 11,063–11,082, doi:10.1029/2000JB900003.